Bull. Soc. géol. Fr., 2010, t. 181, n° 4, pp. 377-390

Subsurface temperature maps in French sedimentary basins: new data compilation and interpolation

DAMIEN BONTÉ[1], LAURENT GUILLOU-FROTTIER[2], CYNTHIA GARIBALDI[2,3], BERNARD BOURGINE[2], SIMON LOPEZ[2], VINCENT BOUCHOT[2] and FRANCIS LUCAZEAU[4]

Key-words. – BHT, Temperature maps, France, Sedimentary basins, 3D thermal model

Abstract. – Assessment of the underground geothermal potential requires the knowledge of deep temperatures (1-5 km). Here, we present new temperature maps obtained from oil boreholes in the French sedimentary basins. Because of their origin, the data need to be corrected, and their local character necessitates spatial interpolation. Previous maps were obtained in the 1970s using empirical corrections and manual interpolation. In this study, we update the number of measurements by using values collected during the last thirty years, correct the temperatures for transient perturbations and carry out statistical analyses before modelling the 3D distribution of temperatures. This dataset provides 977 temperatures corrected for transient perturbations in 593 boreholes located in the French sedimentary basins. An average temperature gradient of 30.6°C/km is obtained for a representative surface temperature of 10°C. When surface temperature is not accounted for, deep measurements are best fitted with a temperature gradient of 25.7°C/km. We perform a geostatistical analysis on a residual temperature dataset (using a drift of 25.7°C/km) to constrain the 3D interpolation kriging procedure with horizontal and vertical models of variograms. The interpolated residual temperatures are added to the country-scale averaged drift in order to get a three dimensional thermal structure of the French sedimentary basins. The 3D thermal block enables us to extract isothermal surfaces and 2D sections (iso-depth maps and iso-longitude cross-sections). A number of anomalies with a limited depth and spatial extension have been identified, from shallow in the Rhine graben and Aquitanian basin, to deep in the Provence basin. Some of these anomalies (Paris basin, Alsace, south of the Provence basin) may be partly related to thick insulating sediments, while for some others (southwestern Aquitanian basin, part of the Provence basin) large-scale fluid circulation may explain superimposed cold and warm anomalies.

Cartographie des températures du sous-sol des bassins sédimentaires français : nouvelles compilation de données et interpolation

Mots-clés. – BHT, Cartes de température, France, Bassins sédimentaires, Modèle thermique 3D

Résumé. – L'évaluation du potentiel géothermique du sous-sol nécessite la connaissance des températures profondes (1 à 5 km). Nous présentons des cartes de température obtenues à partir de données pétrolières mesurées dans les bassins sédimentaires français. L'origine de ces données entraîne la nécessité d'une correction et leur caractère ponctuel requiert une interpolation. Les cartes précédentes, qui datent des années 70, ont été construites à partir de corrections empiriques et d'une interpolation manuelle. La nouvelle base de données contient les données mesurées au cours des trente dernières années, et les données ont été corrigées des perturbations transitoires. Une analyse statistique a été réalisée avant la modélisation 3D des températures. Un total de 977 mesures corrigées est obtenu à partir de 593 forages répartis sur les bassins sédimentaires français. Une analyse statistique a permis de définir un gradient moyen de 30,6 °C/km quand la température de surface de 10 °C est imposée. Si cette dernière n'est pas prise en compte, le meilleur ajustement des données profondes nécessite un gradient de 25,7 °C/km. Ce gradient moyen varie selon le basin sédimentaire considéré, de 27,1 °C/km dans le basin Aquitain à 34,9 °C/km dans le basin de Paris. Une analyse géostatistique a permis de contraindre l'interpolation et le krigeage 3D à partir d'un modèle de variogramme horizontal et vertical. Une dérive verticale à l'échelle du pays ajuste l'augmentation des températures profondes (25,7 °C/km). Cette dérive est soustraite des données BHT corrigées afin d'interpoler les températures résiduelles. Le modèle thermique 3D est alors obtenu en rajoutant la dérive aux résidus interpolés, et permet d'extraire des sections verticales et des cartes isothermes. Un certain nombre d'anomalies sont identifiées, peu profondes dans le graben du Rhin ou dans le bassin Aquitain, et profondes dans le bassin Provençal. Certaines d'entre elles (bassin de Paris, Alsace, une partie du bassin Provençal) pourraient être reliées à l'épaisseur de sédiments isolants, alors que pour le sud-est du bassin Aquitain ou pour une partie du bassin Provençal, des circulations de fluides pourrait expliquer la superposition d'anomalies chaudes et froides.

1. Vrije Universiteit, Faculteit der Aard-en Levenswetenschappen, subafdeling Tektoniek, de Boelelaan 1085, 1081 HV Amsterdam, The Netherlands; damien.bonte@falw.vu.nl
2. BRGM, Mineral Resources Division, 3 avenue Claude Guillemin, BP 6009, 45060 Orléans cedex 2, France
3. Université de Nice, Laboratoire GéoAzur, 28 avenue Valrose, 06108 Nice cedex 2, France
4. Géosciences Marine, Institut de Physique du Globe/CNRS UMR 7154, 4 Place Jussieu, 75252 Paris cedex 05, France
Manuscrit déposé le 20 avril 2009 ; accepté après révision le 21 février 2010.

INTRODUCTION

Interest in geothermal energy has recently increased in relation to global warming and to a rise in oil prices. Geological energy, being both ecological, and independent of seasonal or climatic conditions, represents an alternative to traditional energy sources. Conventional exploitation of geothermal power requires two major conditions to be met: a large quantity of fluid that can circulate in high-permeability rocks (reservoir), and sufficiently high temperatures at depth. According to Lindal [1973], a minimum of 50°C is required to power large-scale heating projects and greenhouse heating. In the case of the Dogger reservoir of the Paris basin, temperatures of 55-85°C (at 1500-2000 m) are exploited for district heating projects [Lemale and Pivin, 1987; Lopez *et al.*, 2010]. In some rare new projects such as Landau (Rhine graben, Germany), the reservoir, consisting of lower Triassic sandstones and its fractured granitic basement, supplies hot fluids (150°C) at 3200 m, and is exploited for electricity (3.8 MWe) [Baumgärtner *et al.*, 2007]. The depths at which rocks may reach a sufficient temperature to produce urban heating or to supply electricity (60-200°C) vary with the regional geological setting, but their optimum is around 3000-3500 m for electricity and around 1500-2000 m for district heating. These conditions are obtained in the French sedimentary basins as they are deep enough, porous and/or fractured, and contain some fluids (fig. 1).

It is clear that temperature maps are of primary interest for the development of new geothermal projects (e.g., electricity production, heating). Public, industrial, and even individual demand is now such that there is a real demand for precise maps of underground temperatures at different depths, depending on individual needs. However, the construction of such maps is limited by the existence and the quality of outdated temperature datasets from the 1970s. As a first preliminary step, this paper presents a new compilation of available deep-temperature data in French sedimentary basins. A geostatistical treatment at country-scale is discussed, and a 3D thermal model is built. Temperature maps are then provided, together with associated uncertainties.

Underground temperature data is mainly measured inside boreholes used for mining or oil exploration. Since this paper is dedicated to moderate to high temperatures (i.e., those at a depth of more than 1 km), and because mining boreholes rarely exceed a few hundred meters in depth, we only consider oil exploration boreholes in this study. For example, heat flow studies generally use temperature measurements performed in mining boreholes because core samples are available and measured temperature profiles are in equilibrium. Because mining boreholes are too shallow for the objectives of this study, they were not included in our database. It follows that temperature maps will be constructed using temperature data located in the French sedimentary basins – namely the Paris basin, the Aquitanian basin, the Provence (or South-East) basin, and other basins belonging to the western part of the European Cenozoic Rift System (Rhine graben, Bresse, Limagne) (fig. 1).

Most of the temperature data recorded in oil exploration boreholes needs to be corrected as thermal equilibrium is not achieved when the measurement is performed. Different correction methods can be used, especially when measurement history is available [e.g., Goutorbe *et al.*, 2007]. In the late 1970s, when subsurface temperature in France was mapped for the first time [Gable, 1978], temporal information was not available. In order to correct temperature data from transient perturbation, Gable [1978] therefore used a statistical correction that was time-independent: two measurements performed at the same depth were assigned the same correction. In the present study, we recompiled all the data available from petroleum boreholes, including measurement history, in order to provide a newly corrected dataset using an analytical methodology [Goutorbe *et al.*, 2007]. Gable [1978] also created his maps manually, with no indication on the contouring procedure. Here, we use a 3D kriging interpolation method constrained by a geostatistical data analysis in order to build a 3D thermal block. The main advantage of this method is its ability to build an associated 3D uncertainty grid.

In this paper, we use recent and improved methodologies to build a 3D thermal block, which is the first step required to extract deliverable 2D maps and cross-sections. The final representation can be a series of iso-depth maps of the subsurface temperature, which can be used during the initial exploration phases of geothermal energy development

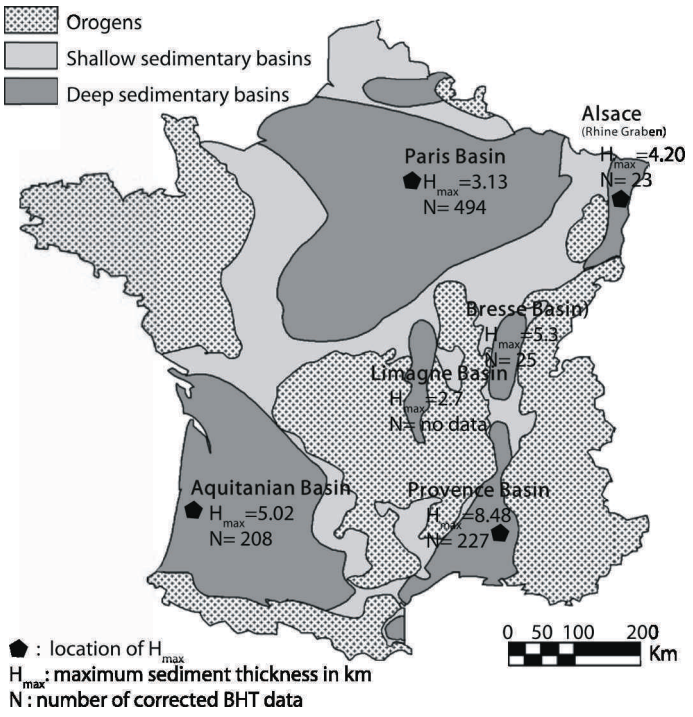

FIG. 1. – Location of the sedimentary basins in France. Crosses: old crystalline basements and recent orogens. Light grey: shallow sedimentary basins. Dark grey: deep sedimentary basins (modified after BRGM). The number of corrected temperature datasets in this study and the maximum thickness (in km) of sedimentary basins are indicated. Locations and values of maximum depths of sediments for the Paris basin, the Aquitanian basin, and the Alsace and Provence basin are taken from Tesauro *et al.* [2008]. Data for Limagne and Bresse basins after Calcagno *et al.* [2008] and Bergerat *et al.* [1990].

FIG. 1. – *Localisation des aquifères profonds et des bassins sédimentaires français. Croix : socle et orogènes récents; gris clair : bassins sédimentaires superficiel; gris foncé : bassins sédimentaires profonds (modifié d'après BRGM). Le nombre des données corrigées dans cette étude et l'épaisseur maximum des bassins sont indiqués. La position et les valeurs maximum des épaisseurs du bassin de Paris, du bassin Aquitain et du bassin de Provence proviennent de Tesauro et al. [2008]. Les données pour la Limagne et la Bresse viennent de Calcagno et al. [2008] et Bergerat* et al. *[1990].*

programs. Temperature maps over geological structures, such as a geological interface for pre-targeted area of interest, can also be extracted from the 3D thermal block. As an example, in this paper we present iso-depth temperature maps in the French sedimentary basins, as well as iso-temperature maps and vertical cross-sections at the country scale.

METHODOLOGY: DATA COMPILATION AND CORRECTIONS

Temperature data in boreholes

As noted above, deep temperature datasets are collected from oil boreholes. Three main kinds of temperatures measurements are available:

– thermometry is a continuous temperature measurement, but in oil exploration boreholes it is used to monitor cementation behind the borehole casing. Since the cementation reaction is exothermic, in-situ temperatures are much higher than equilibrium values. Correction should be possible, but practically, this requires using parameters that are unavailable (e.g., time between cementation and measurements, cementation thickness, type of cement, etc);

– the DST (Drill Stem Test) is a procedure used to test a formation (e.g., pressure, temperature, permeability, etc) in the borehole by pumping the surrounding fluid. By definition, the pumped fluid is in thermal equilibrium with the surrounding formation and DST temperatures do not require any correction;

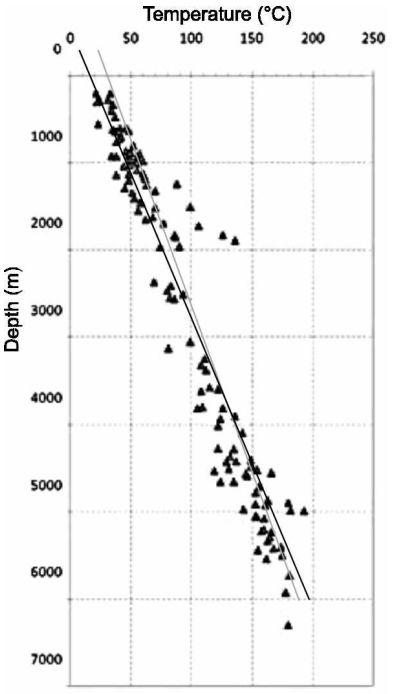

FIG. 2. – Temperature versus depth for DST measurements, which do not require any correction. Black line: best fitting increasing trend when a fixed surface temperature of 10ºC is imposed. Grey line: best fitting linear trend with no additional constraint.
FIG. 2. – *Température en fonction de la profondeur pour les mesures DST qui ne nécessitent pas de correction. La ligne noire montre l'augmentation lorsque la température de surface est imposée à 10 ºC. La ligne grise montre le meilleur ajustement linéaire sans contrainte additionnelle en surface.*

– the BHT (Bottom Hole Temperature) is a side-product of most logging tools. It corresponds to the maximum temperature recorded during logging – theoretically (but not necessarily) the temperature at the bottom. Before logging operations begin, a borehole is cleaned by a circulation of mud to remove cuttings. The mud is injected at a temperature that is usually colder than that of the borehole itself. Because the time elapsing between the end of the mud circulation and the measurement of temperature is usually so short (typically only a few dozen hours), the measured temperature is not at equilibrium, and a correction is required (see § Correction of the BHT).

Among these different temperatures, only BHT datasets are numerous enough to provide the necessary spatial repartition – both horizontally and vertically – to perform 3D mapping in sedimentary basins. In addition, the information required for data corrections is available in the logging headers.

Before presenting a geostatistical analysis of corrected BHT data, we will first present our raw (i.e., uncorrected) data.

Data compilation and statistics

In France, legislation ensures that onshore exploration borehole data can be accessed immediately, while onshore extension and offshore borehole data can be accessed after 10 years. In this study, we systematically collected all accessible data between the 1930s and the present decade and, as a result, we were able to recover DST and BHT temperature measurements from 16840 logging headers, representing a total of 5684 boreholes. DST data represented only 124 measurements within 53 boreholes. When all these DST datasets from France are gathered and reported as a function of depth (fig. 2), we get a bulk vertical temperature gradient trend of 26.1ºC/km when surface temperature is not imposed. If a fixed surface temperature of 10ºC (average surface temperature in France) is imposed, a vertical temperature gradient of 30.1ºC/km is obtained. These rough estimates are made within the basic hypothesis of a linear increase of temperature with depth. These figures are, however, useful to get a large-scale idea of subsurface temperature evolution in the whole country. In addition, BHT data will be corrected at the country-scale, thus involving the use of a single equilibrium geotherm. We will see in the following sections that individual temperature gradients differ from one basin to another.

DST data and corrected BHT data build a set of 997 temperature data points. Their depth distribution, both for the entire country and for each of the three main basins in France, is shown in figure 3. About two-thirds of the data has been measured at depths of between 1000 and 2500 m, implying that this depth range is better constrained than shallower depths (11% of data between 0 and 1000 m). This point will be accounted for in the geostatistical description of the dataset (§ Interpolation of the 3D thermal block).

Correction of the BHT

As mentioned above, the cleaning of boreholes before logging operations significantly disturbs in-situ temperatures. The least affected part is the bottom of the boreholes, since it is perturbed only by the circulation above. Hopefully, when

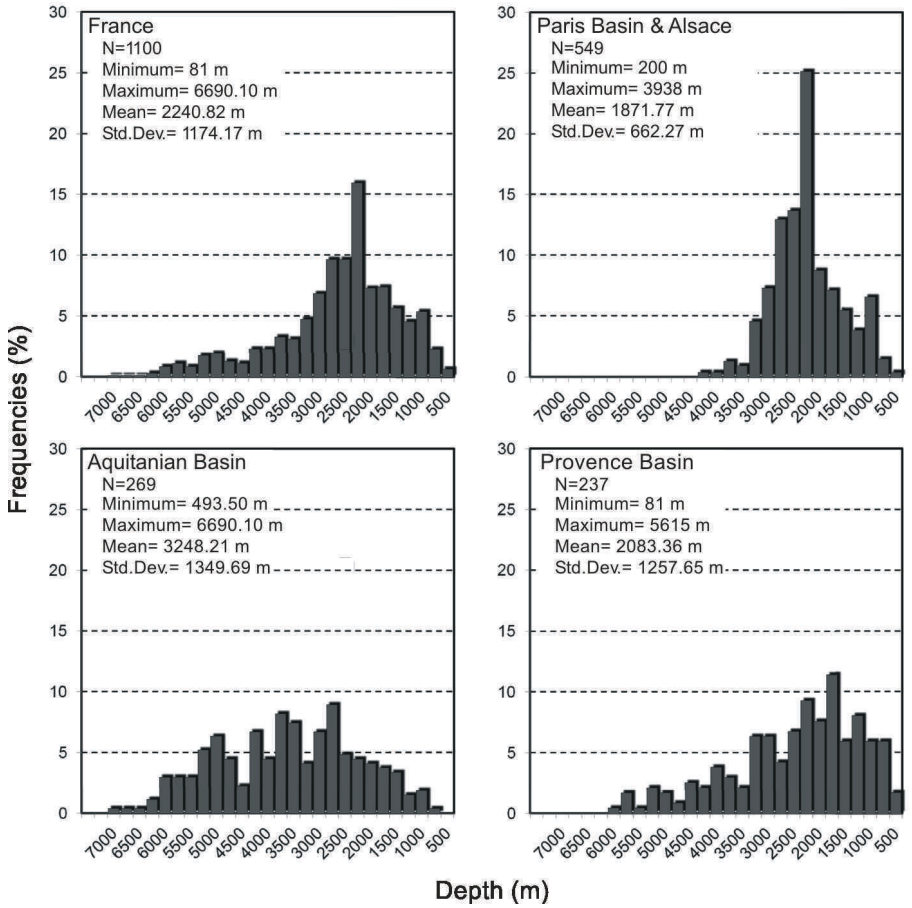

FIG. 3. – Histograms of selected temperature data (DST and corrected BHT data), showing the spread and depth of measurements, across the whole country (top left), and in the three main basins.
FIG. 3. – *Histogramme des données sélectionnées (DST et BHT corrigées), montrant la répartition des données avec la profondeur pour le pays entier (en haut à gauche) et pour les trois bassins principaux.*

this disturbance is well constrained, it is possible to correct the BHT data. Previous authors have proposed a number of different approaches to such correction; we will briefly review certain procedures that can be applied to our dataset in the next section.

Choice of the correction method

Analytical corrections

Several models have been suggested to describe how temperature returns to equilibrium. Analytical corrections are derived from solutions of the transient heat-transfer equation, where mud circulation cooling is simulated by an initial condition either along a line or within a cylinder. In more complex models, mud circulation is considered to last a finite time period.

Existing correction methods have been synthesised by Goutorbe *et al.* [2007]. The different methods result from different hypotheses on the geometry (e.g., line source method, cylinder source method and two-component model), and on the time evolution (e.g., continuous or instantaneous cooling). Unlike the line source method, the cylinder source method can account for a finite width perturbation, while the two-component models recognise in addition the different thermal properties between the borehole mud and surrounding rocks. Borehole radius is used in the equations. In the continuous case, the cold perturbation is defined with a certain time scale (mud circulation time is taken into account). Line source and cylinder source methods can be performed in continuous or instantaneous perturbation time scale. The two-component model takes into account the time scale of the perturbation.

The methods compiled by Goutorbe *et al.* [2007] are the ICS (Instantaneous Cylinder Source), the ILS (Instantaneous Linear Source), the CLS (Continuous Linear Source), the CCS (Continuous Cylinder Source), the Horner (a simplified version of the CLS method) and the two-component model. The two-component model, however, requires many parameters that are rarely available, such as the thermal properties of mud. As a result, we have chosen to reject this method.

The choice between geometric hypotheses for the model (whether line or cylinder source) is driven by the restrictions on the borehole diameter versus the time after circulation. The line source is restricted by the fact that the thermal evolution predicts a time delay equivalent to the time needed for conduction along borehole radius. In other words, if the 'time after circulation' (hereafter noted t_e) is too low, the cold front will not reach the measurement point [see figure 5a in Goutorbe *et al.*, 2007]. This problem can

be avoided by limiting the dataset where $t_e > t_c$, where t_c is the duration of mud circulation. With an averaged borehole radius of 22 cm, and using the associated conductive time-scale, we estimate that the minimum 'time after circulation' t_e should be 5 hours 10 mins. If values with a 'time after circulation' lower than this minimum value are removed from linear methods (ILS and CLS methods), the number of corrected data is significantly decreased (by 29.5% for the ILS method, 14.8% for the Horner method and 13.8% for the CLS method). In order to keep the largest dataset of BHT measurements available for correction, we will not use any linear source methods (including the Horner method which is an approximation of such methods).

The choice of the time evolution hypotheses (instant or continuous source) is determined by the availability of the 'time of circulation' parameter, which is usually not available.

From all these considerations, and because we want to keep the largest dataset without integrating errors, BHT measurements in French sedimentary basins have been corrected with the ICS method presented by Goutorbe *et al.* [2007]. A comparison between the ICS and the other correction methods on the French data reveals that only a limited amount of data shows differences greater than ± 5ºC (fig. 4). Actually, more than 75% of the data corrected with the Horner method has the same value (± 1ºC) as that corrected using the ICS method. Similar percentages are achieved for the ILS, CCS and CLS methods (45%, 60%, and 35% respectively). Practically, the ICS method has two unknown parameters: the energy of the cold source, and the equilibrium temperature we are looking for. Two pairs of (T_{BHT}, 'time after circulation') values at a given depth are thus required to fit the theoretical profile of thermal relaxation.

Statistical correction

When applying the ICS correction method to BHT data from the Provence basin, only 25 temperature datasets can be corrected, whereas 227 sets of BHT uncorrected data are available. This is mainly because the 'time after circulation' was not indicated in most logging headers. Consequently, in order to maintain a satisfactory spatial coverage, a statistical correction method has been applied to the 227 remaining uncorrected data from the Provence basin. In the early 1970s, the AAPG (American Association of Petroleum Geologists) carried out the Geothermal Survey of North America (GSNA), leading to the construction of a massive data base (over 20000 BHT from over 10000 boreholes in the USA). Based on the calibration of BHT data from DST measurements in Oklahoma, Harrison *et al.* [1983] proposed the AAPG statistical correction method (see Deming [1989] for a discussion on empirical correction methods). We first applied this correction to BHT data from the Provence basin. Figure 5 shows the result of the equation 1, a comparison between the two methods (ICS correction for 10 temperature datasets and AAPG correction for all other data).

$$T(z) \quad T_{AAPG} \quad T_{BHT}(AAPG) \quad T_{ICS} \quad \frac{T_{BHT}(ICS)}{n_{BHT}} \tag{1}$$

where T_{AAPG} refers to the temperature corrected using the AAPG method, $T_{BHT}(AAPG)$ to the BHT temperature measurement used for the AAPG correction, T_{ICS} to the temperature corrected using the ICS methods, $\Sigma T_{BHT}(ICS)$ to the sum of the BHT temperatures measurements used for the ICS correction and n_{BHT} to the number of BHT temperatures measurement used to calculate T_{ICS}.

The difference between the two methods has an average value of 3.7ºC, with a maximum of 11.7ºC at 3800 m (fig. 5). With an averaged temperature value of 120-125ºC at 4000 m, this 11.7ºC difference represents less than 10% of absolute temperatures, as is the case at 2000 m (fig. 5). By correcting the remaining 202 BHT data with the

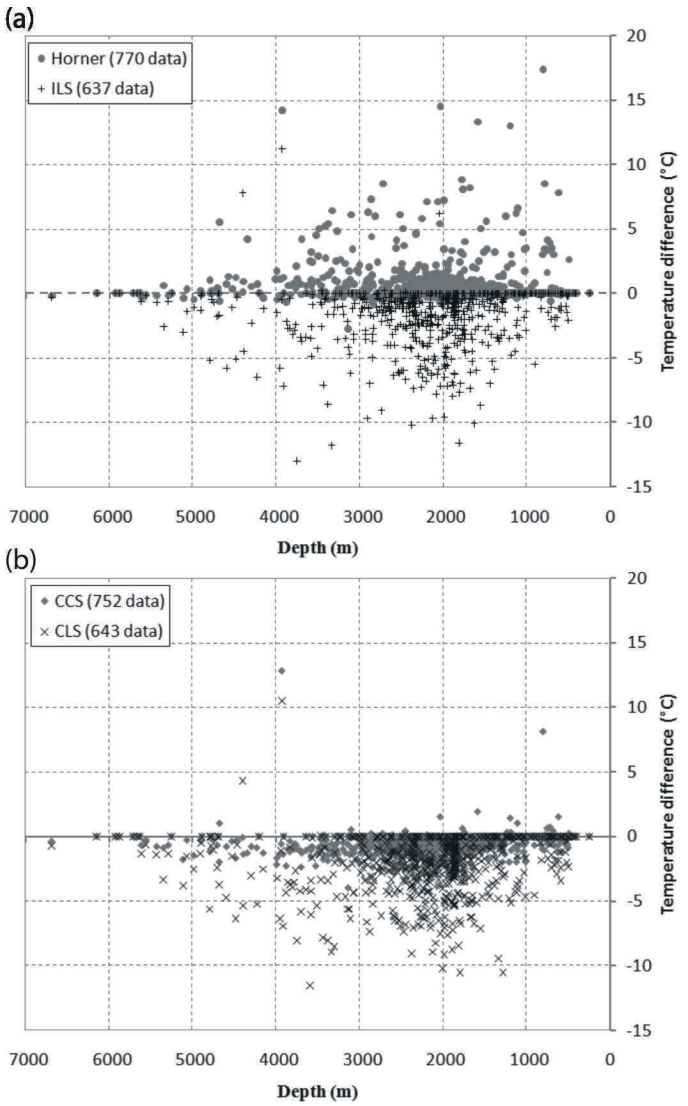

FIG. 4. – Comparison between correction methods as a function of depth. (a) Difference between temperatures corrected with the ICS method and temperatures corrected with the Horner method (dots) and the ILS method (crosses). (b) Difference between temperatures corrected with the ICS method and temperatures corrected with the CCS method (dots) and the CLS method (crosses). Most of the differences belong to the [-1ºC, +1ºC] range. See text for details.

FIG. 4. – *Comparaison entre les différentes méthodes de correction en fonction de la profondeur. (a) Différences entre les températures corrigées avec la méthode ICS et les températures corrigées avec la méthode de Horner (points) et la méthode ILS (croix). (b) Différences entre les températures corrigées avec la méthode ICS et les températures corrigées avec la méthode CCS (points) et la méthode CLS (croix). La plupart des différences ne dépassent pas ± 1 ºC (voir texte pour les détails).*

statistical AAPG method, we were able to get 227 sets of corrected BHT data and 10 sets of DST data.

Uncertainty of BHT correction

As we have discussed above, our objective is to create the largest possible dataset drawn from reliable data. The aim of our corrections is to obtain corrected BHT data that is as close as possible to the formation temperature at thermal equilibrium (before drilling). It is generally accepted that the correction of the BHT data gives an uncertainty of between ± 5-10°C [e.g., Brigaud, 1989; Goutorbe *et al.*, 2007]. As a consequence, uncertainty is relatively high at shallow depths, but may represent only 2-5% of the estimated temperature at a depth of 5 km. This uncertainty range has to be taken into account when using the data.

Corrected dataset

Spatial repartition of temperature data

Corrected BHT data covers a large part of the sedimentary basins in France. However, when compared to the initial uncorrected data repartition (fig. 6), the corrected data has a relatively smaller spatial coverage. In the Paris basin, for example, the northern part only shows one value, and the western part is uncovered, although the central part of the basin has a better covering. In the Aquitanian basin, only the south and the western part are correctly covered. In contrast with these two basins, the Provence basin is well covered by the data because the correction method is different (see previous section). It must be pointed out that if the AAPG correction method had been applied to the entire dataset, a better spatial coverage would have been obtained, albeit with somewhat larger uncertainties at depth (fig. 5).

Temperature repartition with depth

Temperature datasets are mainly available for three large-scale basins: the Paris basin, the Aquitanian basin and the Provence basin. Datasets are also available in small basins related to the Alps. The distribution of temperatures, however, is irregular and obviously depends on basin geometry. Figure 7a highlights some of the differences related to the thickness of each sedimentary basin. While the maximum data depth is around 6000 m in the French Provence basin and in the Aquitanian basin, it is lower than 4000 m in the Paris basin and in the Alpine-related basins (see H_{max} values in figure 1).

The simplest way to characterise the thermal regime of a basin consists of estimating the average temperature gradient. In the plot on the right of figure 6, the surface temperature is fixed at a constant value of 10°C, giving an average temperature gradient of 30.6°C/km for all corrected temperature data (and 28.8°C/km for uncorrected data). When considered separately, each basin shows distinct temperature gradients (fig. 7a). The Provence basin and the Alpine-related basins have an average temperature gradient close to the national value, while the Aquitanian basin has a lower value of 27.1°C /km and the Paris basin has a higher value of 34.9°C/km. These estimates have to be carefully used, since they represent large-scale averages [see Garibaldi *et al.*, 2010, for a detailed analysis of one basin]. Figure 7b illustrates temperature variations around the basin-scale average temperature gradient (residual temperatures). Most of the values are within a range of ± 20°C in the Aquitanian basin and the Paris basin. In the Provence basin, datasets have a larger dispersion, particularly at depths of more than 3000 m, where values can diverge from the average temperature by more than 40°C. At around 3000 m in depth, the maximum temperature difference in the Provence basin exceeds 70°C, whereas in the Aquitanian and Paris basins, this difference stays at around 40°C (38°C and 42°C respectively). This example highlights that extrapolating the temperature of uncovered areas based on average temperature gradient can yield unrealistic temperatures. To limit potential errors made through rough extrapolation, and to control interpolation, it is therefore necessary to perform a geostatistical analysis of the entire dataset.

It is also remarkable that the shallower parts of the datasets in the Paris, Aquitanian and Provencal basins show a low temperature gradient (see upper part of figure 7a). This implies a high temperature in comparison to a standard geotherm, which would start at 10°C with an evolution of

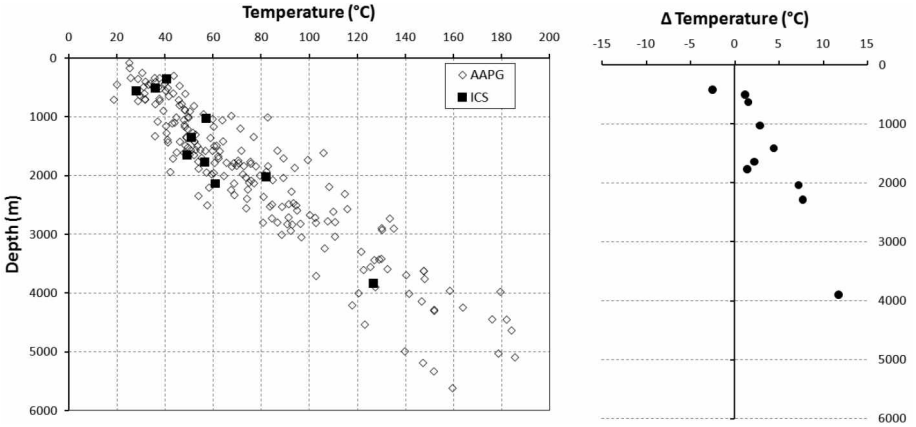

FIG. 5. – Corrected data in the Provence basin. (a) Temperature versus depth; black squares: BHT data corrected with the ICS method. Diamonds: BHT data corrected with the AAPG method. (b) The temperature difference between the two corrections to the BHT measurement (shown by dots). See text for details.

FIG. 5. – *Données corrigées dans le bassin de Provence.* (a) *Température en fonction de la profondeur ; Carrées noirs : données BHT corrigées avec la méthode ICS ; losange : données BHT corrigées avec la méthode AAPG.* (b) *La différence entre les deux corrections par rapport aux BHT mesurées (points). Voir texte pour les détails*

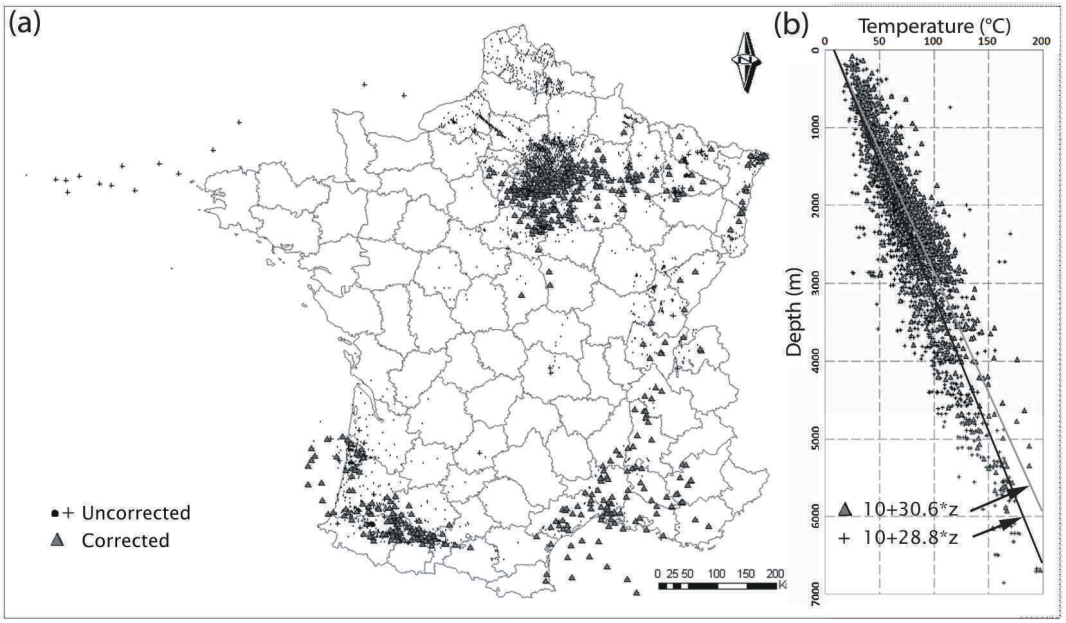

FIG. 6. – Location of oil exploration boreholes in France. Dots: uncorrected BHT data. Grey triangles: corrected BHT data. (a) Spatial repartition of oil boreholes in France. (b) Temperature of the BHT data as a function of depth. Black line: trend for the uncorrected BHT measurements. Grey line: trend for corrected BHT data when a fixed surface temperature of 10°C is imposed.
FIG. 6. – *Position des forages pétroliers en France. Points : données non corrigées, triangles gris : données corrigées.* (a) *Répartition spatiale des forages ;* (b) *Température en fonction de la profondeur. Ligne noire : tendance linéaire pour les données non corrigées ; ligne grise : tendance pour les données corrigées, lorsqu'une température de 10 °C est imposée en surface.*

30°C per km. One of the explanations for this effect could be that the injected drilling mud is, at shallow depths, at a higher temperature than the drilled formation. This would lead to the formation being heated instead of cooled, as is usually assumed for the correction of the BHT.

INTERPOLATION OF THE 3D THERMAL BLOCK

Pre-process on the dataset

Once the dataset has been built, it can then be used for the interpolation and extrapolation required to construct a 3D thermal block. We chose to compute the 3D thermal block for the entire country based on our entire dataset in order to avoid distinction between basins and get an average thermal behaviour of the entire country. On the other hand, local analyses can be carried out using the associated local dataset [e.g., Garibaldi *et al.*, 2010].

Temperatures at different depths cannot be directly compared because of the intrinsic drift in the vertical direction. The entire dataset was therefore used to compute the best fitting linear increasing trend, thus representing the vertical drift in the entire dataset. This linear increasing trend corresponds to a first order approximation, and could, of course, be refined by a polynomial vertical drift accounting for lithological variations [e.g., Chiles and Gable, 1984]. In contrast to previous local analyses (fig. 7), the top surface was not assigned a fixed temperature value, as this enabled us to give a more important weight to the depth range where numerous values are present (see § Data compilation and statistics and figure 3). The residual temperatures T_{res} and the obtained vertical drift T_{drift} can be expressed as:

$$T_{residual} \quad T_{BHTc} \quad T_{drift} \tag{2a}$$

with

$$T_{drift} \quad 0.0247 \quad z \quad 23.137 \tag{2b}$$

where T_{BHTc} corresponds to corrected BHT data at depth z. This vertical drift (represented by the dashed line in figure 8a) is closer to the deep temperature-increasing trend since it is not constrained by a fixed surface temperature. Our aim in choosing the deeper values to constrain our gradient is also motivated in part by the uncertainty of the BHT correction (between 5-10°C), which in proportion gives a lower uncertainty with increased depth. Since the analysis of deeper temperatures is favoured here, the vertical drift of equation 2b is used. The result of this modification is a dataset formed from residual temperatures (fig. 8b) computed with this single country-scale drift described in equation 2.

Geostatistical analysis: the variogram

The experimental variogram

The understanding of a dataset in which the values are randomly positioned can be made using an experimental variogram [Clark, 1979; Chilès and Delfiner, 1999]. The variogram is defined by a correlation, represented by the variogram value ($\gamma(h)$) versus the distance between two values (h). As described by Chilès and Delfiner [1999], calculation of the variogram, $\gamma(h)$, for $N(h)$ pairs of measured values ($z(x_i)$, $z(x_i+h)$) at distance of h is given by:

$$(h) \quad \frac{1}{2} \frac{\sum_{i\ 1}^{N(h)} z(x_i) \quad z(x_i \quad h)^{\ 2}}{N(h)} \tag{3}$$

To take into account the 3D data repartition, particularly because the horizontal and vertical scales differ by 2 orders of magnitude, the experimental variogram is composed of two variograms, one horizontal and one vertical (broken lines, figures 9a and 9b respectively).

The experimental horizontal variogram (fig. 11a, broken line) shows an inhomogeneous repartition. Indeed, for the first 200 km, the variogram has a smooth aspect that can be related directly to the correlation of values in the same basin. Beyond 300 km, however, the high variability of the variogram indicates that correlation is obtained from data belonging to distinct basins. Figure 11b shows the experimental vertical variogram. The horizontal and vertical variograms have the same nugget effect and sill, but different ranges.

The model of variogram

In order to use the features of the obtained experimental variograms in the interpolation procedure, a mathematical model of the experimental variograms is required. Several models are available; the most commonly used are summarised by Chilès and Delfiner [1999]. For every model, three parameters are important: the nugget effect, the sill and the range. The nugget effect corresponds to the value of the variogram when h tends to zero; it defines the non-repetitiveness of the measurements at the same point, or the local variance. The sill is related to a stationary regime, in which the value distribution is random when this value is reached. The sill is graphically related to a plateau in the curve. The range corresponds to the distance at which the variogram reaches the sill. When an experimental variogram trend cannot be perfectly fitted by a single variogram model, a plurimodel of variogram can be used.

Figures 9a and 9b include the chosen models of variograms (red curves). They are composed of four structures: a pure nugget effect and three spherical models. From the experimental variograms, the nugget effect is chosen to be 25^oC^2, and the horizontal range is around 400 km (fig. 9a) whereas the vertical range is only 2 km (fig. 9b). Such a large horizontal range involves pairs of data from separate sedimentary basins, which could be criticized and could be due to the simple linear drift chosen to be the same all over the studied area. To reproduce experimental observations, ranges of the theoretical models are chosen anisotropically to reflect this higher correlation on larger distances along horizontal directions. The values of the parameters for each variogram model are summarised in table I.

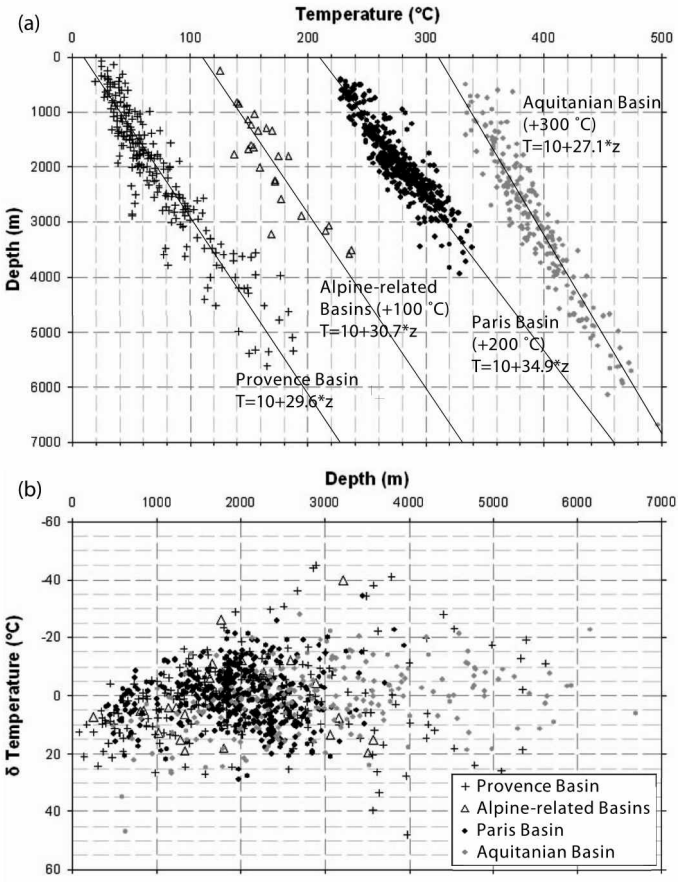

FIG. 7. – Corrected BHT temperature data with depth, separated per basin. (a) The averaged geotherm, with a fixed surface temperature of 10°C, is indicated. To demonstrate results more clearly, temperatures of a given basin are shifted by 100°C with respect to previous basins. (b) Residual temperatures computed with the individual geotherms indicated in (a).
FIG. 7. – *Données BHT corrigées en fonction de la profondeur pour chaque bassin.* (a) *Le géotherme moyen, où la température moyenne de 10 °C est imposée en surface, est indiqué. Pour une meilleure lisibilité, les températures d'un bassin donné sont décalées de 100 °C par rapport à celles du précédent bassin.* (b) *Températures résiduelles calculées avec les géothermes individuels indiqués en a).*

TABLE I. – Parameters describing the vertical and horizontal variograms of figure 9.
TABL. I. – *Paramètres décrivant le variogramme horizontal et le variogramme vertical de la figure 9.*

			Anisotropic range (in m)		
Structure #	**Basic structure**	**Sill**	**U**	**V**	**W**
1	Nugget Effect	25			
2	Spherical Model #1	20	10000	10000	2200
3	Spherical Model #2	27	70000	70000	2200
4	Spherical Model #3	95	450000	450000	2000

Interpolation of the 3D thermal block

In order to perform the interpolation, space has to be divided into grids. The global grid size is 7 km vertically, and 800 km × 1200 km in E-W and N-S directions, respectively. The mesh size is 50 m vertically and 2 km ×2 km horizontally. The top of the grid is dictated by surface topography.

The chosen method for statistical interpolation is kriging. The theory of kriging (originally developed by Krige [1951]) was developed by Matheron [1963] for geological use, based on the assumption of spatial relations between data. The interpolation is controlled by two main parameters: the variogram discussed above, and the neighbourhood. We used a 'simple neighbourhood' method where the maximum distance for the interpolation is controlled by the variogram range. Because the kriging is 3D, a tolerance thickness is accepted for the interpolation. Practically, this means that for the interpolation from a grid node, the two

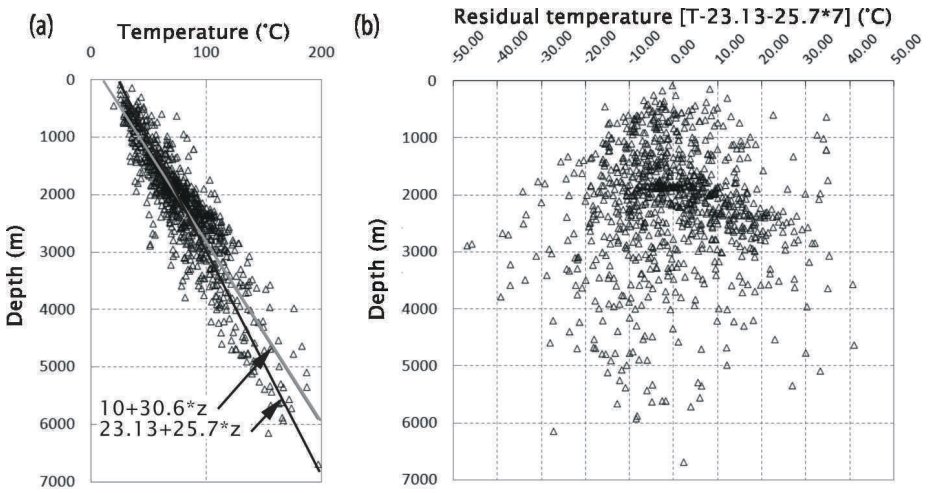

FIG. 8. – Vertical drifts and residual temperatures for the entire dataset. (a) Two vertical drifts can be defined, one with an imposed surface temperature of 10ºC, the other without imposing a surface temperature (black line). (b) Residual temperatures taking the best-fitting drift of deep temperatures (black line in a) as a reference.

FIG. 8. – *Dérives verticales et températures résiduelles pour l'ensemble des données.* (a) *Deux dérives peuvent être définies, l'une avec une température de surface de 10 ºC, l'autre sans imposer de température en surface (ligne noire).* (b) *Températures résiduelles en prenant comme référence la dérive qui ajuste au mieux les températures profondes (ligne noire en a).*

directions (horizontal and vertical) are not single line/plan, but instead correspond to a certain thickness.

In order to obtain a 3D thermal block showing temperature in the subsurface of the French sedimentary basins, the 3D grid has to be implemented with the previously removed drift, since the 3D grid has been built with the residual temperatures. In the non-sedimentary areas (below and outside basins), the same averaged geotherm (equation 1b) was imposed. Figure 11a shows the obtained 3D thermal block. This representation highlights the need to illustrate temperature variations by slices through the 3D block.

DISCUSSION ON THE RESULT OF THE 3D THERMAL BLOCK

In the following, above-average temperature values will be described as positive anomalies and below-average temperature values as negative anomalies.

Generic representation

To view the results obtained by the 3D block, the block has been sliced according to horizontal iso-depth (fig. 10a-e) and vertical iso-longitude (fig. 11). These temperature map

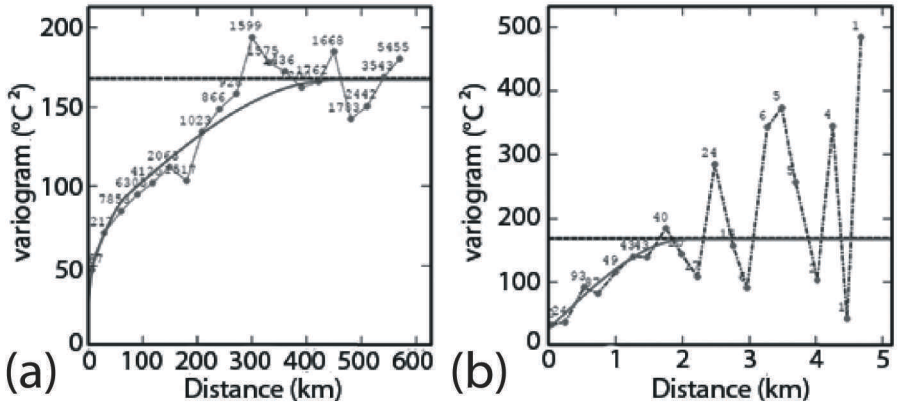

FIG. 9. – Variograms used (in $^oC^2$) for the 3D interpolation (see text for details): (a) horizontal variogram; (b) vertical variogram. Figures represent the number of pairs used to compute the variogram.

FIG. 9. – *Variogrammes utilisés (en $^oC^2$) pour l'interpolation 3D (voir les détails dans le texte).* (a) *Variogramme horizontal ;* (b) *variogramme vertical. Les figures représentent le nombre de paires utilisées pour construire le variogramme.*

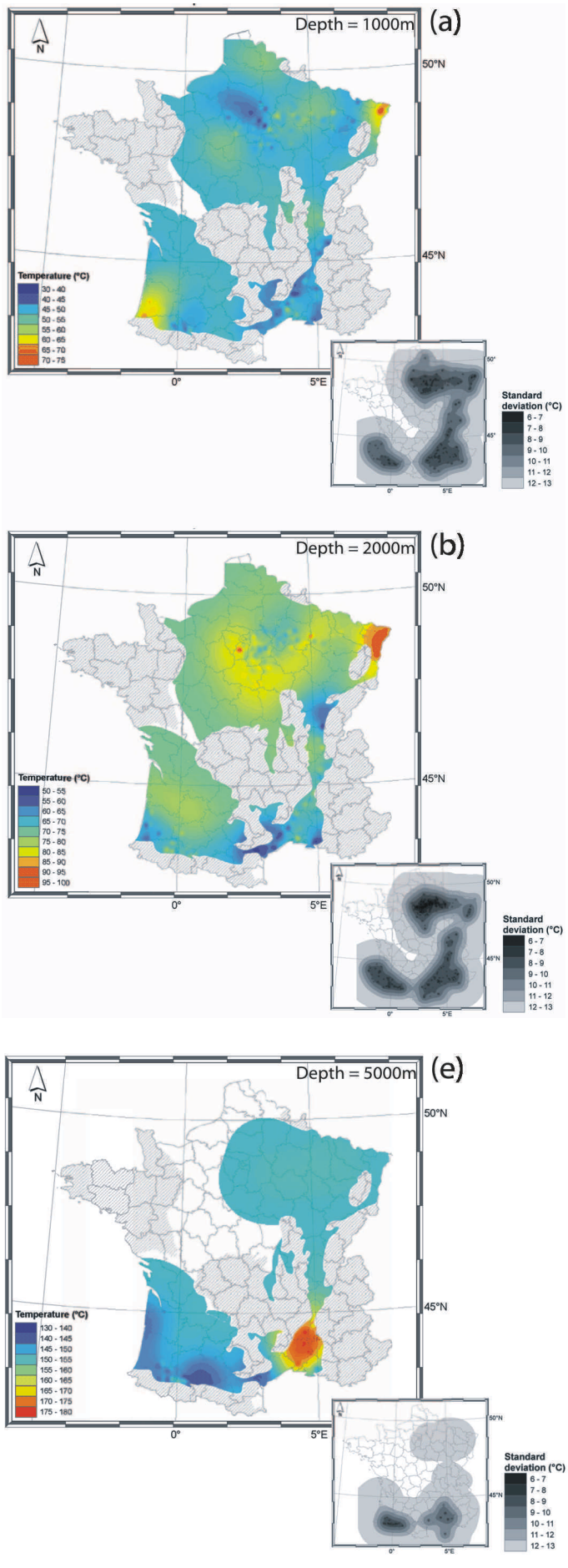

FIG. 10. – Iso-depth (a: 1000 m, b: 2000 m, c: 3000 m, d: 4000 m, e: 5000 m) horizontal slices in the 3D thermal block. At each depth, the colour map represents the temperature and the small black and white map gives the standard deviation of the temperatures. Hatched areas represent orogens.

FIG. 10. – *Coupes horizontales (cartes iso-profondeur) dans le bloc thermique 3D* (a : *1000 m,* b : *2000 m,* c : *3000 m,* d : *4000 m,* e : *5000 m). Pour chaque profondeur, la carte en couleur représente les températures, et la carte en noir et blanc les écart-types sur les températures. Les zones hachurées correspondent aux orogènes.*

anomalies have been built from the average vertical drift in France as inferred from equation 2 (i.e., a vertical drift of 25.7°C/km), and not from the average temperature gradient constrained by a fixed surface temperature (e.g., the 30.6°C/km value).

The horizontal iso-depth slices presented in this work show temperature maps every 1000 m, from 1000 m to 5000 m. The zero reference for the iso-depth map is the ground surface. Topographic variations may lead to significant changes in temperature gradient at a depth of 1 km, but only when small-scale and high-amplitude relief is present [Blackwell *et al.*, 1980]. This is not the case for our present study, since datasets are measured in sedimentary basins where a smooth topography prevails. In order to obtain the most reliable result, we have tried to avoid extrapolation, and for this reason, the maximum iso-depth map is 5000 m. Figure 7 indicates the maximum depth of the data in each basin: the Provence Basin and Aquitanian Basin have values greater than 5000 m, whereas the Paris Basin values are less than 4000 m. In order to deliver a complete thermal characterisation of the subsurface in French sedimentary basins, the iso-depth temperature maps are completed with maps of standard deviation inherent to the interpolation method (bottom-right parts of figures 10a-e).

The Rhine graben

One of the most remarkable anomalies in France is located in Alsace (northeast area). This anomaly is well-known thanks to the European geothermal project of Soultz-sous-Forêts [Gérard *et al.*, 2006]. Temperatures measured in the Soultz boreholes [Schellschmidt and Clauser, 1996] indicate a high gradient in the first kilometre (over 100°C/km), decreasing from 1000 m to 2000 m (around 30°C/km), and becoming very low below 2000 m (under 20°C/km). This evolution could be explained by a combination of several effects, including (i) a thermal insulation effect due to the slightly lower conducting sediments [Schwarz and Henk, 2005], (ii) a large-scale fluid circulation in the permeable zones of the granite roof, which brings hot fluids beneath the sedimentary cover [Sanjuan *et al*, 2006], (iii) a significant heating effect due to the anomalously high radioactive content of the granite [Royer and Danis, 1988] and (iv) a thinning of the crust due to the Oligocene rifting [Brun *et al*, 1992]. As expected, our temperature maps show a localised high positive anomaly in the northern part of the French Rhine graben at 1000 m depth (fig. 10a) and a larger anomaly at 2000 m depth (fig. 10b). The reason that this anomaly remains present at a depth of 2000 m is probably due to the fact that even if the gradient has decreased between 1000 m and 2000 m, the temperature is still higher than average as a result of the very high gradient in the first kilometre (> 100°C/km). In addition, it must be recalled that the vertical variogram used for the interpolation of the 3D thermal block influences the interpolation until 2000 m. This is confirmed with the next maps (fig. 10c-e) where temperatures can be seen to recover the average surrounding values.

The Paris basin

A quick examination of the iso-depth maps (fig. 10) and the slice taken from the 3D model (fig. 11b) in the Paris basin reveals a major positive anomaly in the centre of the basin at 3000 m (fig. 10c and fig. 11b), with maximum values up to 120°C. It must be noted that at this depth, the yellow areas of figure 10c do not belong to the basin anymore while most of the orange and red zones are still within the basin. The intensity of this positive anomaly decreases at 2000 m and even becomes a negative anomaly in some areas with regard to the average temperature value of 70°C (fig. 10b). The origin of this anomaly at 3000 m, and its evolution both under and above this depth can be attributed to (i) the sediment thickness, (ii) the type of sediments and their thermal

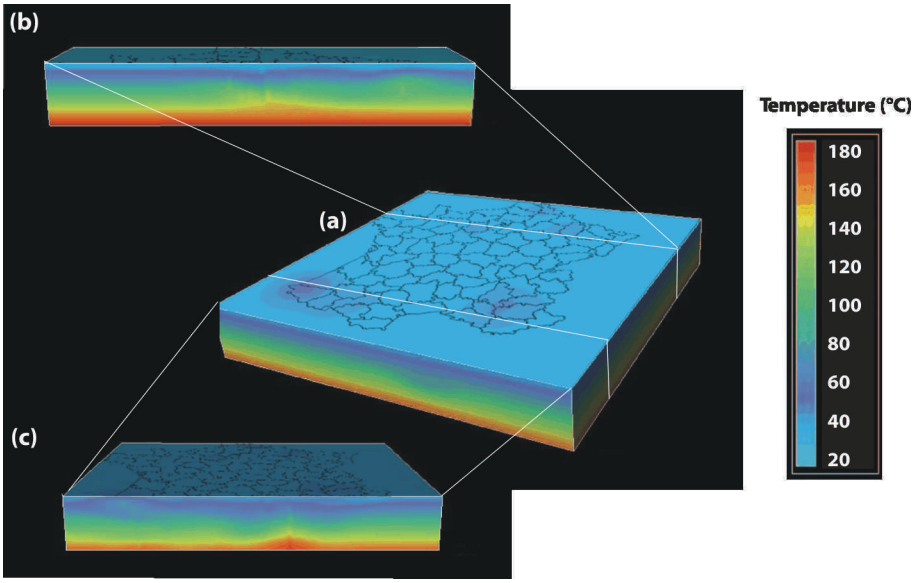

FIG. 11. – Vertical slices in the 3D thermal block. The thickness of the block is 6000 m. (a) 3D thermal block showing the location of the slices. (b) Vertical slice from southern Aquitanian basin to Provence basin. (c) Vertical slice from western France to Alsace areas crossing the central part of the Paris basin.
FIG. 11. – *Coupes verticales dans le bloc thermique 3D. L'epaisseur du bloc thermique 3D est de 6000 m.* (a) *bloc 3D montrant la localisation des coupes ;* (b) *coupe verticale allant du sud du bassin Aquitain au bassin de Provence ; (c) coupe verticale allant de l'ouest de la France à l'Alsace en traversant la partie centrale du bassin de Paris.*

properties, (iii) the impact of the basement composition on radiogenic heat production, and (iv) the water circulation in the basin. The role of water circulation within the basin – either topographically-driven or density-driven – may indeed not be negligible, since estimated Darcy velocities would be around 0.3 m per yr [Wei *et al.*, 1990], which is greater than the minimum computed values in up- and down-flow zones of convecting systems in sedimentary basins [Simms and Garven, 2004]. In addition, Menjoz and Lambert [1991] suggested that the positive thermal anomaly, south of Paris (fig. 10b), corresponds to a mixing zone between two distinct fluid circulation pathways within the Dogger aquifer.

The general sediment thickness in the Paris basin takes the shape of a bowl: thicker in the centre and thinner around the edges [Dercourt, 2002]. A number of studies have discussed the thermal conductivity in sedimentary rocks [e.g., Clark, 1966; Schön, 1996; Allen and Allen, 2005] and have given values that range from 1.5 W m^{-1} K^{-1} (shale) to 4 W m^{-1} K^{-1} (sandstone). In the basement, typical values are usually between 2-4 W m^{-1} K^{-1} [Allen and Allen, 2005]. In the Paris basin, the Lias is partly related to a marine environment (paleo-bathymetry over 200 m) and deposition is composed of shale [Le Solleuz, 2003], which has a low thermal conductivity. The combined insulating effect of this shale layer and its maximum burial at the centre of the Paris basin (top of the formation at ~ 2500 m) might be the major cause in explaining the positive anomaly that is visible at 3000 m (fig. 10c). As emphasized by Vasseur *et al.* [1995], additional subtle effects due to anisotropy of thermal conductivity of shale may also play a role in the spatial distribution of thermal anomalies.

In addition, the parameters of the Paris basin basement can be described by the surrounding massifs [Ziegler *et al*, 2004; Burg *et al*, 1994]. Within the Massif Central, the emplacement of granite has been dated between 360 and 295 Ma [Faure *et al.*, 2009]. Lefort and Agarwal [1996] as well as Galdeano and Guillon [1988] studied the basement of the Paris basin using gravimetric methods, and placed particular emphasis on the presence of granites in the basement because two of these granites are cartographically localised within the 3000 m positive anomaly. Studies of the radiogenic heat production of the granites in the surrounding massif of the Paris basin have given values of 2.13-5.80 μW m^{-3} for the Massif Central [Lucazeau *et al.*, 1984] and 3.73-4.62 μW m^{-3} for Brittany [Jolivet *et al.*, 1989]. If we compare these figures to the values of 1.27-2.34 μW m^{-3} usually assumed for the upper crust [e.g., Lucazeau *et al.*, 1984] it would appear that these high radiogenic granites are a part of the visible positive anomaly at 3000 m.

It therefore seems likely that the positive anomaly identified at a depth of 3000 m in the central part of the Paris basin can be understood as the combined effect of localised granites that produce more radiogenic heat than the surrounding metamorphic rocks, and of an insulating effect resulting from the bulk thickness of the sediments within the basin, reinforced by the proportion of shales in sedimentary layers. Temperature for deeper values are difficult to assess: the Paris basin has a maximum depth of 3130 m [Dewolf and Pomerol, 2005], and there are consequently very few BHT measurements available below 3000 m. Any temperature variation below 3000 m is therefore not well constrained.

The Aquitanian basin

The southwestern part of the Aquitanian basin shows a major positive anomaly at 1000 m depth with values over 65°C. This anomaly becomes negative when a depth of 2000 m is reached with the same range of temperatures as occurs at 1000 m (fig. 10a and fig. 10b) and lower. The slice of the 3D model presented in figure 11c, provides us with a view of the shape of this system: the high temperature comes from the east, below the department of Gers, and extends upwards and westwards to create the positive anomaly at a depth of 1000 m. In other words, the temperature gradient in the southwestern Aquitanian basin seems to be very low between 1000 and 2000 m.

We have identified two possibilities underlying this anomaly. The first possibility concerns a potential imprecision in the BHT correction, due to the heating of the formation and mud drilling at a shallow depth. This effect was also suggested above (§ Temperature repartition with depth) to explain the general increase of temperature at shallow depth; but in that case, the intensity of the anomaly and the inversion of temperature at higher depth could also have

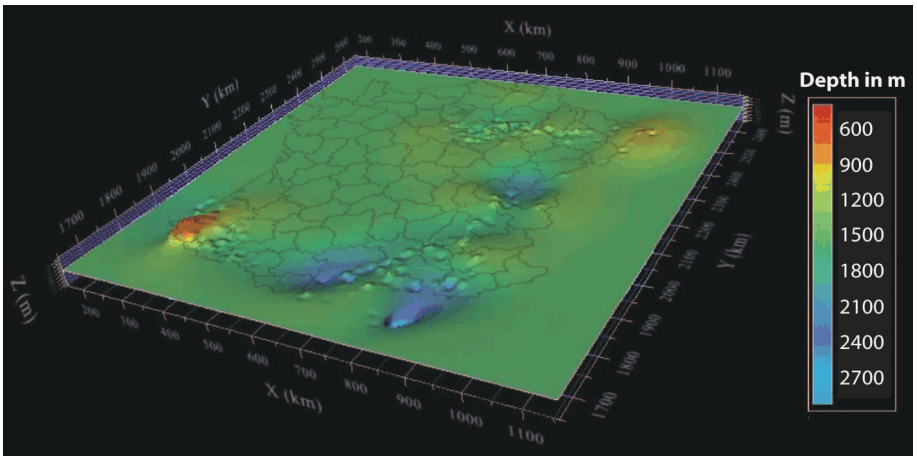

FIG. 12. – Iso-temperature map (60°C) of the thermal block.
FIG. 12. – *Carte isotherme (60 °C) issue du bloc thermique 3D.*

had another cause. A second possibility stems from the fact that the Aquitanian basin is well known for its aquifers [e.g., Bourgine *et al.,* 1999; Seguin, 2003; Douez, 2007] some of which (e.g., the Palaeocene aquifer) covering the area under discussion. It is therefore possible that some fluid circulation could take place, creating a convection current that drags heat upwards from a depth and carries it to a shallower part of the basin. This possible bulk convecting fluid circulation would indeed create positive anomalies at shallow depths and negative anomalies below, thus explaining the establishment of a low temperature gradient.

Another positive anomaly has been identified in the central-west part of the Aquitanian basin. The intensity of this anomaly is smaller than the more southerly one discussed above, but its development is potentially related to the northern part of the Palaeocene aquifer discussed by Bourgine *et al.* [1999].

The Provence basin

The Provence basin shows small extensions of both negative and positive anomalies at depths of 1000 m and 2000 m (fig. 10a and fig. 10b). These anomalies appear to be aligned on a southwest northeast trend. Garibaldi *et al.* [2010] have described these anomalies in relation to the Cevennes and Nîmes faults. The most important of these deep anomalies is visible on the south of France section (fig. 11c) as well as on the iso-depth maps at 4000 m and 5000 m (fig. 10d and fig. 10e). Based on the conclusions of Garibaldi *et al.* [2010], this high amplitude anomaly can be seen to be related to the Vistrenque Basin, and is probably due to the combined effects of a thick sedimentary cover and insulating sediments.

Specific use

In addition to the plane slices presented in the previous section, the 3D thermal block can be sliced following parameters other than depth or latitude/longitude. For geothermal use, iso-temperature maps can be made.

The iso-temperature map of figure 12 has been made from the 3D thermal block at a temperature of 60°C. This representation is useful for determining favourable areas for district heating projects. At the scale of France, the average depth for this temperature is 1430 m (green areas). Important shallower values can be identified in Alsace and in the southwestern part of the Aquitanian basin. In Alsace, this anomaly is related to the processes listed above. In the Aquitanian basin, the effect has also been observed in figure 11, but its intensity appears to have been underestimated by the chosen vertical cross-section. Indeed, this iso-temperature map shows that temperatures of 60°C can be reached at depths lower than 500 m in the southwestern part of the Aquitanian basin. The central part of the Paris basin also shows a positive (albeit lower temperature) anomaly. The negative anomalies showing temperatures of 60°C at deeper depths have to be considered with caution since they are all constrained by a small number of temperature values.

CONCLUSION

The main objective of this paper was to present a new temperature database of the first kilometres beneath French sedimentary basins. From this database we can make a number of distinct choices. Firstly, geostatistical analysis of the entire dataset can be based on the choice of two specific variograms, the horizontal one being described by three spatial structures with sills ranging from 20-95 km. Any other spatial structure that fits this experimental variogram can obviously be chosen, involving possible different interpolation parameters during the kriging procedure. Secondly, a 3D thermal block covering all sedimentary basins of France was constructed by using residuals computed from a large-scale increasing trend of temperature-depth data. This trend enables a better fit of deep temperatures when compared with a trend constrained by a constant surface temperature of 10°C. Since temperature maps are constructed with the aim of identifying anomalies with respect to surrounding temperatures, this choice was considered more relevant for geothermal applications than any other trend.

Analysis of temperature anomalies on a countrywide-scale (fig. 10, fig. 11 and fig. 12) reveals anomalous zones within a restricted depth range, which is probably related to the maximum depth of any associated basins. For example, the positive (warm) anomaly in the Paris basin is located where sediment thickness is the largest (compare fig. 10c and fig. 1). The negative (cold) anomaly of the Provence basin changes to a warm anomaly from 4000 m to 5000 m depth, where sedimentary rocks are still present (fig. 1 and fig. 10e). However, it must be noted that fluid circulation within aquifers may also be invoked to explain specific features such as unexpected low temperature gradients within a given depth range (e.g., south-west of Aquitanian basin).

If, as seems to be the case, the large-scale features of temperature anomaly are indeed related to sediment thickness, smaller scale distribution must be investigated with local geostatistical data analyses. In this case, local variograms may differ greatly from those presented in figure 9, allowing small-scale geological features to be decipherable in the spatial description of a local dataset. An example of such a restricted dataset (using a proper variogram) is presented in Garibaldi *et al.* [2010].

Acknowledgements. – This study was supported by the BRGM and the Vrije Universiteit of Amsterdam. It corresponds to an improved version of Damien Bonté Master's thesis. We are very grateful to the BEPH (Bureau Exploitation-Production des Hydrocarbures) for the access to the logs header of petroleum boreholes. We appreciated the comments of J.-L. Rudkiewicz and of the anonymous reviewer. A grateful thanks to Rosie Marshall for the correction of the English. This is BRGM publication 06341.

References

ALLEN P.A. & ALLEN J.R. (2005). – Basin analysis: principles and applications. – 2nd edition, Oxford Blackwell Pub, 549p.

BAUMGÄRTNER J., MENZEL H. & HAUFFE P. (2007). – The geox GmbH Project in Landau. – The First Geothermal Power Project in Palatinate / Upper Rhine Valley, at *First European Geothermal Review.* – Geothermal Energy for Electric Power Production, Mainz, Germany.

BERGERAT F., MUGNIER J.-L., GUELLEC S., TRUFFERT C., CAZES M., DAMOTTE B. & ROURE F. (1990). – Extension tectonics and subsidence of the Bresse basin: a view from Ecors data. – *Mém. Soc. géol. France*, **156**, 145-157.

BLACKWELL D., STEELE J.L. & BROTT C.A. (1980). – The terrain effect on terrestrial heat flow. – *J. Geophys. Res.*, **85**, 4757-4772.

BOURGINE B., CAPDEVILLE J.P., LACI-IASSAGNE P., SCHOEN R., SEGUIN J.-J. & SOURISSEAU B. (1999). – Outil de gestion des systèmes aquifères du Sud du bassin Adour-Garonne. Base de données géoréférencées et modèle conceptuel. – Rapport BRGM R 40633, 42p

BRIGAUD F. (1989). – Conductivité thermique et champ de température dans les bassins sédimentaires à partir des données de puits. – Thèse de doctorat, Univ. Montpellier 2, 414p.

BRUN J.-P., GUTSCHER M.-A. & ECORS-DEKORP teams (1992). – Deep crustal structure of the Rhine Graben from DEKORP-ECORS seismic reflection data: a summary. *In*: P.A. ZIEGLER, Ed., Geodynamics of rifting, Vol. I. Case history studies on rifts: Europe and Asia. – *Tectonophysics*, **208**, 139-147.

BURG J.-P., VAN DEN DRIESSCHE J. & BRUN J.-P. (1994). – Syn- to post-thickening extension in the Variscan belt of western Europe: mode and structural consequences. – *Géol. France*, **3**, 33-51.

CALCAGNO P., BAUJARD C., DAGALLIER A., GUILLOU-FROTTIER L., GENTER A., KOHL T. & COURRIOUX G. (2008). – 3D geological modelling and geothermal assessment of the Limagne basin (France). – *Internat. Geological Modelling Conference GeoMod2008*, 22-24 September 2008, Firenze, Italy

CHILES J.-P. & DELFINER P. (1999). – Geostatistics: modeling spatial uncertainty – Wiley, Chichester, 720p.

CHILES J.-P. & GABLE R. (1984). – Three dimensional modelling of a geothermal field. *In*: G. VERLY *et al.*, Eds, Geostatistics for natural resources characterization, part 2. – D. Reidel Publish. Comp., Hingham, MA, 587-598.

CLARK S.P. (1966). – Thermal conductivity. *In*: S.P. CLARK, Ed., Handbook of physical constants. – *Geol. Soc. Amer. Mem.*, **97**, 459-482.

CLARK S.P. (1979). – Practical geostatistics. – Elsevier, Amsterdam, 137p.

DEMING D. (1989). – Application of bottom-hole temperature corrections in geothermal studies. – *Geothermics*, **18**, 775-786.

DERCOURT J. (2002). – Géologie et géodynamique de la France (outremer et européenne). – Dunod, Paris, 3rd edition, 230 p.

DEWOLF Y. & POMEROL C. (2005). – The Parisian Basin. *In*: E.A. KOSTER, Eds, The physical geography of western Europe. – Oxford University Press, 251-266.

DOUEZ O. (2007). – Réponse d'un système aquifère multicouche aux variations paléoclimatiques et aux sollicitations anthropiques – Approche par modélisation couplée hydrodynamique, thermique et géochimique. – Thèse de doctorat, Université de Bordeaux 3, 306p.

FAURE M., LARDEAUX J.-M. & LEDRU P. (2009). – A review of the pre-Permian geology of the Variscan French Massif Central. – *C. R. Geoscience*, **341**, 202-213.

GABLE R. (1978). – Acquisition et rassemblement de données géothermiques disponibles en France. – BRGM report 78 SGN 284 GTH, 60p.

GALDEANO A. & GUILLON J.C. (1988). – Interprétation des données magnétiques et gravimétriques. *In*: M. CAZES et G. TOREILLES, Eds, Etude de la croûte terrestre par sismique profonde – Profil Nord de la France, structure hercynienne. – Ed. Technip, Rueil.

GARIBALDI C., GUILLOU-FROTTIER L., LARDEAUX J.-M., BONTÉ D., LOPEZ S., BOUCHOT V. & LEDRU P. (2010). – Relationship between thermal anomalies, geological structures and fluid flow: new evidence in application to the Provence basin (southeast France). In: D. GASQUET, J.-Y. JOSNIN and Y. LAGABRIELLE, Eds. Hydrothermalisme en domaine continental – *Bull. Soc. géol. Fr.*, **181**, 4, 363-376.

GERARD A., GENTER A., KOHL T., LUTZ P., ROSE P. & RUMMEL F. (2006). – The deep EGS (Enhamced Geothermal System) project at Soultz-sous-Forêts (Alsace, France). – Geothermics, 35, 473-483.

GOUTORBE B., LUCAZEAU F. & BONNEVILLE A. (2007). – Comparison of several BHT correction methods: a case study on an Australian data set. – *Geophys. J. Int*, **170,** 913-922.

HAINING R.P. (2003). – Spatial data analysis: theory and practice. – Cambridge: Cambridge University Press, 432 p.

HARRISON W.E., LUZA K.V., PRATER M.L. & CHUENG P.K. (1983). – Geothermal resource assessment of Oklahoma. – *Oklahoma Geol. Surv., Spec. Publ.*, **83-1**, 42 p.

JOLIVET J., BIENFAIT G., VIGNERESSE J.-L. & CUNEY M. (1989). – Heat flow and heat production in Brittany (western France). – *Tectonophysics,* **159**, 61-72.

KRIGE D. (1951). – A statistical approach to some basic mine valuation problems on the Witwatersrand. – *J. Chem., Metal. Mining Soc. of South Africa,* **52**, 119-139.

LE SOLLEUZ A. (2003). – Modélisation thermo-mécanique et stratigraphique de la genèse et de l'évolution d'un bassin sédimentaire intraplaque: le bassin de Paris. – Thèse de doctorat, Université Paris 6, 225 p.

LEFORT J.-P. & AGARWAL B.N.P. (1996). – Gravity evidence for an Alpine buckling of the crust beneath the Paris Basin. – *Tectonophysics*, **258**,1-14.

LEMALE J. & PIVIN M. (1987). – La filière géothermique – Premier bilan. – AFME, Paris, France 2nd édition, 80p.

LINDAL B. (1973). – Industrial and other applications of geothermal energy. *In*: Geothermal energy: Review of research and development. – UNESCO, Paris, LC No. 72-97138, 135-148

LOPEZ S., HAMM V., LE BRUN M., SCHAPER L., BOISSIER F., COTICHE C. & GIUGLARIS E. (2010). – 40 years of Dogger aquifer management in Ile-de-France, Paris Basin, France. – *Geothermics* (in press).

LUCAZEAU F., VASSEUR G. & BAYER R. (1984). – Interpretation of heat flow in the French Massif Central. – *Tectonophysics*, **103**, 99-120.

MATHERON G. (1963). – Principles of geostatistics. – *Econ. Geol.*, **58**, 1246-1266.

MENJOZ A. & LAMBERT M. (1991). – Hydrodynamique des aquifères profonds et incidence des effets de densité. – *Hydrogéologie*, **4**, 311-320.

ROYER J.J. & DANIS M. (1988). – Steady state geothermal model of the crust and the problem of the boundary conditions: application to a rift system, the southern Rhinegraben. – *Tectonophysics*, **156**, 239-255**.**

SANJUAN B., PINAULT J.-L., ROSE P., GERARD A., BRACH M., BRAIBANT G., CROUZET C., FOUCHER J.-C., GAUTIER A. & TOUZELET S. (2006). – Tracer testing of the geothermal heat exchanger at Soultz-sous-Forêts (France) between 2000 and 2005. – *Geothermics*, **35**, 622-653.

SCHELLSCHMIDT R. & CLAUSER C. (1996). – The thermal regime of the upper Rhine graben and the anomaly at Soultz. – *Z. Angew. Geologie*, **42**, 40-44.

SCHÖN J. (1996). – Physical properties of rocks: Fundamentals and principles of petrophysics. *In*: K. HELBIG and S. TEITEL, Eds, *Handb. Geophys. Explor.,* Sect. 1., vol. 18. – Pergamon, Oxford, U.K.

SCHWARZ M. & HENK A. (2005). – Evolution and structure of the Upper Rhine Graben: insights from three-dimensional thermomechanical modelling. – *Int. J. Earth Sci.*, **94**, 732-750

SEGUIN J.-J. (2003). – Outil de gestion des aquifères du Sud du Bassin Adour-Garonne – Année 4. Calage du modèle hydrodynamique en régime transitoire. – Rapport BRGM/RP-52014-FR.

SIMMS M.A. & GARVEN G. (2004). – Thermal convection in faulted extensional sedimentary basins: theoretical results from finite-element modeling. – *Geofluids*, **4**, 109-130.

TESAURO M., KABAN M.K. & CLOETINGH S.A.P.L. (2008). – EuCRUST-07: a new reference model for the European crust. – *Geophys. Res. Lett.*, **35**, L05313.

VASSEUR G., BRIGAUD F. & DEMONGODIN L. (1995). – Thermal conductivity estimation in sedimentary basins. – *Tectonophysics*, **244**, 167-174.

WEI H.F., LEDOUX E. & DE MARSILY G. (1990). – Regional modelling of groundwater flow and salt and environmental tracer transport in deep aquifers in the Paris basin. – *J. Hydrology*, **120**, 341-358.

ZIEGLER P.A., SCHUMACHER M.E., VAN WEES J.D. & CLOETINGH S. (2004). – Post-Variscan evolution of the lithosphere in the Rhine Graben area: Constraints from subsidence modelling. – *Geol. Soc., London, Spec. Publ.,* **223**, 287-315.